INORGANIC CHEMISTRY FRONTIERS

RESEARCH ARTICLE

View Article Online
View Journal | View Issue

Cite this: *Inorg. Chem. Front.*, 2025, **12**, 2334

Robust high-spin Fe^{2+} centers in 2D TCNQ-based metal–organic frameworks†

Yan Yan Grisan Qiu, *[a] Simone Mearini, [a] Daniel Baranowski, ‡[a] Iulia Cojocariu, [b] Matteo Jugovac, [b] Giovanni Zamborlini, [c,d] Pierluigi Gargiani, [e] Manuel Valvidares, [e] Vitaliy Feyer *[a,f] and Claus Michael Schneider [a,f,g]

Received 6th December 2024,
Accepted 24th January 2025

DOI: 10.1039/d4qi03123g

rsc.li/frontiers-inorganic

Two-dimensional metal–organic frameworks (2D MOFs) are atomically thin materials that combine the properties of organic molecules with the structural characteristics of crystalline inorganic solids. Their unique magnetic and electronic properties arise from the interaction between transition metal centers and organic linkers. This study focuses on the high-spin Fe^{2+} centers in a 7,7,8,8-tetracyanoquinodimethane (TCNQ)-based 2D MOF, where hybridization between Fe 3d states and π-symmetric orbitals of TCNQ ligands stabilizes regularly spaced magnetic centers. X-ray magnetic circular dichroism (XMCD) measurements confirm the robustness of these magnetic properties across various substrates, including graphene and gold.

Introduction

The pursuit of distinct magnetic properties in surface-supported, well-defined metal centers remains a key challenge in materials science.[1] While metal adatoms can provide single-atom magnetism, arranging them into ordered arrays presents substantial difficulties.[2] Additionally, the inherent interactions with substrates often result in the quenching of magnetic moments, thereby limiting their utility.[3,4] In contrast, embedded transition metal (TM) centers in two-dimensional (2D) metal–organic frameworks (MOFs) offer a scalable and robust solution for achieving stable magnetic behavior on surfaces.[5–12]

A notable example of this approach is reported for Fe-terephthalic acid (TPA) complexes deposited on Cu(100).[5] The network morphology is significantly affected by the Fe : TPA stoichiometry, the symmetry as well as the reactivity of the Cu(100) substrate, whereas the thermal annealing allows to stabilize a high-spin (HS) state configuration with a strongly localized Fe^{2+} character. The HS state of Fe^{2+} ions, with four unpaired electrons, results in a relatively high magnetic moment compared to many other TMs. This, in turn, can enhance magnetic interactions between metal centers, strengthening the over ferromagnetic order of the framework.[9–11]

To stabilize the magnetic behavior of these systems, the choice of the substrate plays a critical role.[13,14] In this context, inert substrates minimize direct chemical interactions between the MOF and the surface.[15] As a consequence, the intrinsic properties of the structure can be preserved. Compared to the highly reactive Cu(100) substrate,[5] it is possible to stabilize the HS configuration of Fe^{2+} within the framework on an inert substrate, significantly enhancing the development of robust MOFs.

In this study, we investigate the stabilization of regularly spaced HS Fe^{2+} centers coordinated by 7,7,8,8-tetracyanoquinodimethane (TCNQ) ligands on two weakly interacting substrates, graphene/Ir(111) (Gr/Ir(111)) and Au(111). These 2D MOFs not only provide a robust platform for tailored magnetic properties, but also demonstrate how strong coordination bonds between Fe ions and TCNQ ligands promote hybridization mechanisms between the Fe 3d states and the π-symmetric orbitals of the molecular linker. X-ray magnetic circular dichroism (XMCD) confirms that this MOF-specific coordination environment ensures the stability of unique magnetic properties, even in the presence of different substrates. Ultimately, the arrangement of HS Fe^{2+} centers in well-defined 2D arrays presents advanced opportunities for organometallic-

[a]*Peter Grünberg Institute (PGI-6), Forschungszentrum Jülich GmbH, 52425 Jülich, Germany. E-mail: y.grisan@fz-juelich.de, v.feyer@fz-juelich.de*
[b]*Physics Department, University of Trieste, 34127 Trieste, Italy*
[c]*Institute of Physics, NAWI Graz, University of Graz, 8010 Graz, Austria*
[d]*Department of Physics, TU Dortmund University, 44227 Dortmund, Germany*
[e]*ALBA Synchrotron Light Source, 08290 Barcelona, Spain*
[f]*Faculty of Physics and Center for Nanointegration Duisburg-Essen (CENIDE), University of Duisburg-Essen, 47048 Duisburg, Germany*
[g]*Department of Physics and Astronomy, UC Davis, Davis CA 95616, USA*
†Electronic supplementary information (ESI) available. See DOI: https://doi.org/10.1039/d4qi03123g
‡Present address: Physical and Computational Sciences Directorate and Institute for Integrated Catalysis, Pacific Northwest National Laboratory, Richland, Washington 99354, USA

based electronics and spintronics devices, reinforcing the potential of these MOFs in next-generation magnetic materials.

Results and discussion

The Fe-TCNQ MOFs on Gr/Ir(111) and Au(111) substrates are prepared following the growth protocol described by Jakub *et al.*[15] They employed scanning tunneling microscopy (STM), low-energy electron diffraction (LEED), and density functional theory (DFT) calculations to characterize the structural and electronic properties of the MOF.[15] These studies revealed that the lateral arrangement of the 2D TCNQ-based MOFs is surface-dependent. Specifically, on Gr/Ir(111) the weak interactions between the Fe-TCNQ network and the substrate enable the ligands to adopt a quasi-tetrahedral, nonplanar configuration around the Fe centers. In contrast, on Au(111) the van der Waals (vdW) interactions with the surface draw the Fe ions closer to the surface, resulting in an in-plane displacement of the metal centers, thus planarizing the MOF.[15]

Although STM and LEED data are not included in this work, the identical growth protocols ensure that the Fe-TCNQ frameworks studied here are consistent with the well-characterized structures reported by Jakub *et al.*[15,16] On the basis of these structural insights, the effects of geometric variations on the electronic and magnetic properties of Fe-TCNQ MOFs, supported by Gr/Ir(111) and Au(111), are here explored experimentally. This is particularly significant for understanding the spin and oxidation states of the Fe centers within these frameworks. To address this gap, we perform X-ray absorption spectroscopy (XAS) and XMCD measurements at the Fe $L_{3,2}$-edges. These experiments are employed to comprehensively probe the bonding and the magnetic properties of TM ions in TCNQ-based MOFs, thereby enhancing our understanding of how the substrate influences these properties.

Fig. 1a and b display the XAS spectra with p- and s-polarized light collected across the Fe $L_{3,2}$-edges for the Fe-TCNQ MOFs on both Gr/Ir(111) (red line) and Au(111) (blue line) substrates. The Fe coverage is estimated to be 0.04 ML (with respect to the Au(111) substrate) for both networks.

Given that the embedded Fe centers resemble a surface-diluted system, a comparison with an appropriate reference system is necessary.[5,10,11] This aims to confirm that the signal in the spectra of the Fe MOF is not originating from Fe cluster species that may have formed after the deposition of Fe on the pristine TCNQ layer. Therefore, after depositing an equivalent amount of Fe impurities directly onto the pristine Gr/Ir(111) substrate (Fig. S1†), a detailed comparison of the XAS line shapes between Fe MOF and Fe impurities reveals differences. While the Fe/Gr/Ir(111) spectrum displays broad L_3 and L_2 peaks characteristic of the metallic behavior[17,18] and no sign of linear dichroism, the spectra for the Fe MOF show a pronounced narrowing of features and a well-defined multiplet structure. In particular, these differences in line shapes between the two systems indicate changes in the local electronic environment of the Fe centers, resulting from coordination with the cyano groups of the TCNQ ligands within the MOF. This assumption is further supported by N K-edge XAS spectra, where a notable intensity reduction of π*-type resonances is observed for both Fe MOFs on Gr/Ir(111) and Au(111) surfaces relative to the self-assembled TCNQ molecules on their respective supports (Fig. 2). Specifically, upon Fe deposition, the peaks at 396.9 eV and 398.9 eV of the π-type orbitals (solid red and blue lines) are completely quenched, while the intensity of the resonance associated with the in-

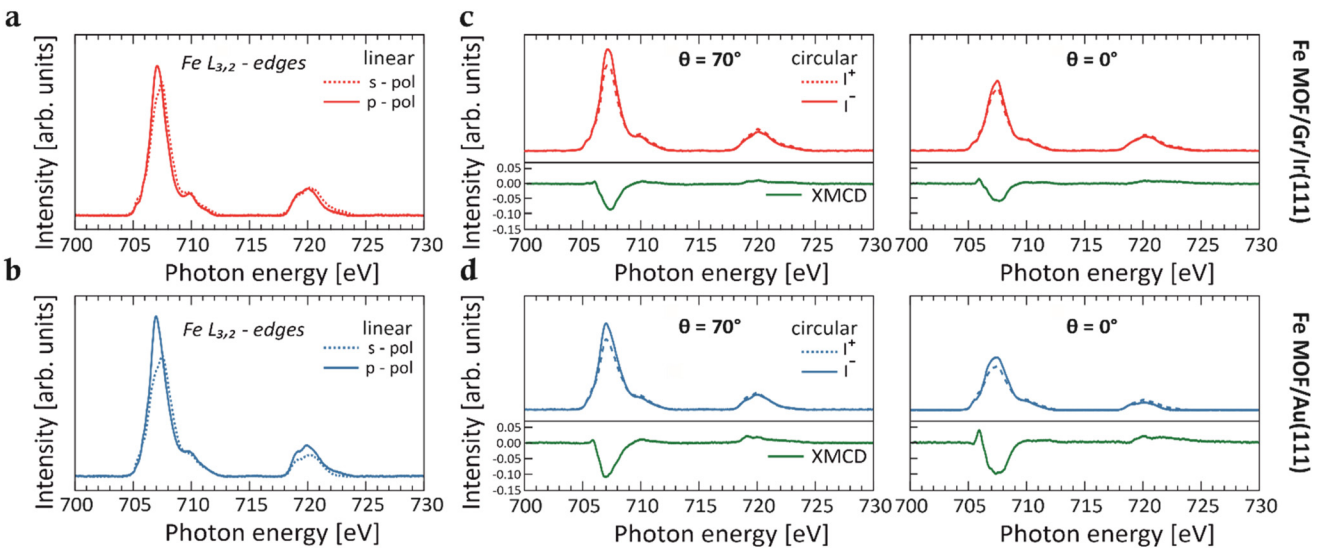

Fig. 1 XAS spectra recorded across the Fe $L_{3,2}$-edges of (a) Fe MOF/Gr/Ir(111) (red line) and (b) Fe MOF/Au(111) (blue line) systems, with s-polarized (s-pol, θ = 70°, dashed line) and p-polarized (p-pol, θ = 70°, solid line) light. (c) and (d) XAS spectra at the Fe $L_{3,2}$-edges of left- (I^-, solid line) and right- (I^+, dashed line) hand circularly polarized light (θ = 70° and θ = 0°, B = 6 T) and resulting XMCD signal (normalized by the corresponding L_3-integrated XAS intensity, green line) for (c) Fe MOF/Gr/Ir(111) and (d) Fe MOF/Au(111) systems. A spline background has been subtracted.

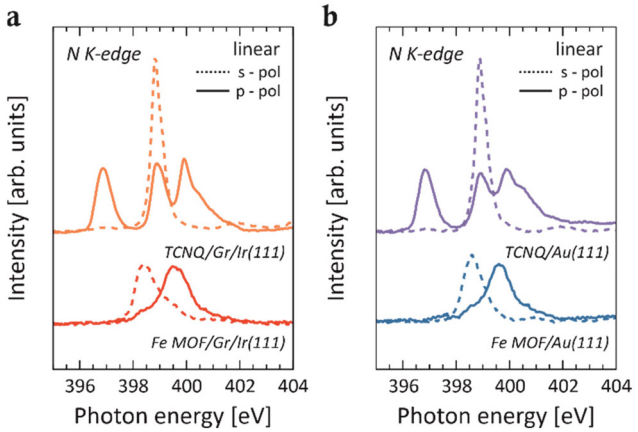

Fig. 2 XAS spectra recorded across the N K-edge of (a) TCNQ/Gr/Ir (111) (orange line) and Fe MOF/Gr/Ir(111) (red line) systems and (b) TCNQ/Au(111) (purple line) and Fe MOF/Au(111) (blue line) systems, with s-polarized (s-pol, θ = 0°, dashed line) and p-polarized (p-pol, θ = 70°, solid line) light.

plane π*-type orbitals (dashed red and blue lines) is substantially reduced. These spectral characteristics offer a clear spectroscopic evidence of the metal–organic coordination and are consistent with those observed for Fe ions coordinated by organic ligands (see Fig. 1), thus suggesting a Fe^{2+} oxidation state.[5,10] Additionally, the strong intensity of resonances observed in the XAS spectra measured across $L_{3,2}$-edges with both p- and s-polarized light is consistent with the HS configuration of Fe^{2+} ions, where unpaired electrons are present in both out-of-plane and in-plane 3d orbitals, allowing for dipole 2p → 3d transitions. Previous DFT calculations[15] support the Fe^{2+} HS quintet state in the Fe-TCNQ frameworks as the most stable configuration on both substrates and show that the local structural environment of the Fe centers influences the energy level alignment. Therefore, this leads to slight variations in the width of the main peak and in the intensity in the XAS spectra at the Fe $L_{3,2}$-edges measured for the MOFs on both substrates, as reported in Fig. 1.

The neutral Fe atom has an electronic configuration of Fe^0 as [Ar] $3d^64s^2$. Summarizing the interpretation of the N K-edge and Fe $L_{3,2}$-edges data, we propose that in the Fe-TCNQ system with 1 : 1 stoichiometry, the Fe^{2+} ions donate two electrons to the TCNQ LUMO, resulting in the formation of doubly charged TCNQ anions. The Fe^{2+} ions are, therefore, stabilized in the [Ar] $3d^6$ configuration. The hybridization in this system plays a crucial role in determining the electronic configuration of the Fe ions and the overall electronic structure of the Fe-TCNQ framework. Indeed, this hybridization leads to the formation of hybrid states primarily composed of Fe 3d and TCNQ orbitals, with some contribution from Fe 4s orbitals.[15] Moreover, in the MOF, the TCNQ gas-phase states and Fe 3d orbitals are reordered due to metal–organic bonding, while the Fe 4s orbitals remain unoccupied.

To understand the magnetic properties of the Fe centers within the MOFs supported by Gr/Ir(111) and Au(111), we conducted XMCD experiments. The XMCD signals were obtained at a maximum magnetic field of 6 T across the Fe $L_{3,2}$-edges, as shown in Fig. 1c and d. Different measurement geometries were set at photon incidence angles of θ = 0° (normal), θ = 54.7° (magic angle), and θ = 70° (grazing) with respect to the surface normal. XMCD measurements performed at various incidence angles provide insights into the alignment of Fe magnetic moments relative to the X-ray incidence direction, revealing the magnetic anisotropy of Fe centers in TCNQ-based MOFs.

As illustrated in Fig. 1c and d, comparing XMCD intensities at θ = 0° and θ = 70° show that Fe centers in TCNQ-MOF on Gr/Ir (111) exhibit weak anisotropy, with higher XMCD intensity observed in the grazing geometry. Remarkably, when these TCNQ-based MOFs are supported on Au(111), a more interacting substrate,[15] the in-plane anisotropy remains almost unchanged. This finding indicates that the Fe-TCNQ coordination bonds effectively stabilize the magnetic orientation, preserving the anisotropy direction across substrates with varying interaction strengths. This result highlights the robustness of the Fe-TCNQ MOF compared to other reported 2D MOF structures.[10]

A similar dominant in-plane magnetic anisotropy within the Fe centers was observed in the above-mentioned Fe-TPA MOFs stabilized on Cu(100). However, adsorption of axial ligands at the Fe sites within this MOF induced a sudden reorientation, rotating the Fe easy axis out of plane.[5] Conversely, the XMCD measurements of 2D Fe-DCA (9,10-dicyanoanthracene) MOF on Au(111) substrate revealed a strong out-of-plane anisotropy in the Fe centers, suggesting that the Au(111) surface has a significant impact on the observed magnetism.[10] Notably, the variations in magnetic anisotropy among these Fe-containing MOFs can be attributed to axial interactions involving the Fe d_{z^2} orbital,[5,15] particularly through direct substrate binding, as observed with Au(111). These findings highlight the role of external chemical environments and substrate properties in modulating the magnetic behavior of Fe centers within the Fe-TPA and Fe-DCA MOFs. In contrast, the results of the Fe-TCNQ MOF emphasize the robustness of this framework, which retains its magnetic anisotropy even when interfaced with the Au(111) substrate.[10]

By applying the sum rules analysis to the XAS and XMCD spectra[5,21,22] collected at multiple incidence angles θ, we quantitatively determine the orbital and the effective spin magnetic moments for the 2D Fe MOFs supported on Gr/Ir(111) and Au (111) substrates (Fig. S2†). Notably, at the so-called "magic angle" configuration (θ = 54.7°), the intra-atomic dipole spin moment is vanishing, permitting a direct determination of the isotropic spin moment. However, as Stepanow *et al.*[23] showed, this approximation may not hold in highly anisotropic environments similar to that of Fe-DCA MOFs.[10] The L_3/L_2 branching ratio in the range of ~4.1–4.6 observed in the Fe-TCNQ MOFs XAS spectra (Fig. 1a and b) is consistent with values reported for HS Fe^{2+} configurations (S = 2) and contrasts with the smaller ratios typically observed for intermediate- or low-spin configurations of Fe^{2+}.[24,25] Furthermore, the spectral shapes of the XAS spectra are similar to those observed for the HS Fe^{2+} in Fe-TPA

MOF.[5] Therefore, our analysis assumes the nominal number of four holes in the 3d orbitals to derive the orbital and effective spin moments. The deduced values in the respective geometries for the different MOFs on Gr/Ir(111) and Au(111) substrates are summarized in Table S1.† The isotropic spin moments (measured at magic angle) for both Fe MOFs on Gr/Ir(111) and Au(111) are evidently underestimated compared to the expected absolute values for Fe^{2+} in the HS configuration. However, despite this discrepancy, the analysis of the calculated magnetic moments reveals a consistent trend for the angular dependence across the two frameworks, with comparable values, thereby confirming similar magnetic responses. Notably, the magnetic moment of Fe MOF on Gr/Ir(111) is smaller than that on Au (111). This behavior can be attributed to the differences in Fe–N bond lengths (~2.08 Å on Au(111) and ~2.04 Å on Gr/Ir(111)),[15] which influence the ligand field strength and the energy level alignment of the Fe 3d orbitals, consequently affecting the magnetic moments. Additionally, the trend of the magnetization curves (Fig. S3†) clearly indicates that even at 6 T, the magnetization is far from saturation, contributing to the underestimation of the magnetic moments and their variation across different substrates. Distinctly, different trends are observed in the XMCD spectra and magnetization curves for Fe impurities on Au(111) (Fe/Au(111)),[10] thus highlighting the influence of the hybridization between the Fe 3d states and the MOs of the organic linker in the Fe-TCNQ network. This hybridization can weaken the magnetic interactions and hinder the full spin alignment, even under high magnetic fields. Therefore, the Fe centers in these MOFs behave as nearly independent paramagnetic units.[11] Furthermore, while the linear response of the system seems to rule out any ferromagnetic coupling between the Fe ions, the possibility of an antiferromagnetic correlation between the Fe spins cannot be excluded.[8]

To gain further insights into the hybridization mechanism between Fe 3d states and the MOs of TCNQ ligands, induced by the coordination bonds and crucial for stabilizing the Fe^{2+} HS configuration, we acquired the valence band (VB) spectra using a photoelectron emission microscope (PEEM).[26] The VB spectra were collected for the Fe MOFs supported on both Gr/Ir(111) and Au(111) substrates, along with the TCNQ self-assembled layers and the bare substrate references, as shown in Fig. 3.

The VB spectrum of TCNQ/Gr/Ir(111) shows a prominent feature at a binding energy (BE) of around 3.0 eV. This feature is attributed to the highest occupied molecular orbital (HOMO) of TCNQ. In contrast, the HOMO peak is not observed in the TCNQ/Au(111) spectrum due to the pronounced contribution of the Au 5d states, which dominates the spectral region (>2 eV) where TCNQ molecular orbitals should typically appear.

The absence of charge transfer from both Gr/Ir(111) and Au (111) substrates to the adsorbed TCNQ molecules is supported by the N K-edge data collected for the pristine TCNQ layer (Fig. 2), whose shapes resemble those of the decoupled molecular system.[27] This interpretation aligns with the current VB data, which show no molecule-related features in the low BE region, typically associated with charge transfer phenomena from the substrate.[28–30]

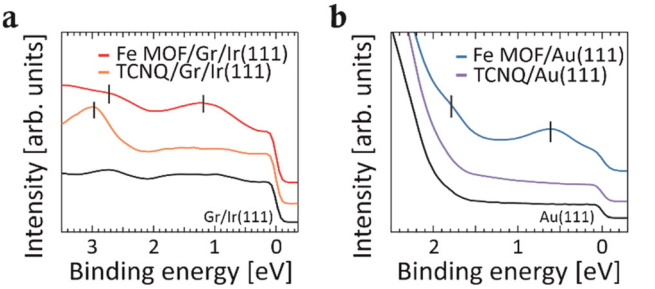

Fig. 3 Momentum-integrated VB spectra recorded for (a) Gr/Ir(111) (black line), TCNQ/Gr/Ir(111) (orange line), Fe MOF/Gr/Ir(111) (red line) and (b) Au(111) (black line), TCNQ/Au(111) (purple line), Fe MOF/Au(111) (blue line).

In order to better visualize these hybridizations, we plot energy *vs.* momentum maps along the high-symmetry direction $\bar{K}-\bar{\Gamma}-\bar{M}$ of the surface Brillouin zone of Gr/Ir(111) and Au(111) for the Fe MOFs using p-polarized light (Fig. 4a and b respectively). Upon Fe deposition on the TCNQ layer (*i.e.*, the formation of the MOF) on both Gr/Ir(111) and Au(111) substrates, distinct new features emerge in the low BE range. Notably, pronounced peaks appear at BEs of approximately 1.2 eV and 2.6 eV on Gr/Ir(111) and 0.6 and 1.8 eV on Au(111). Consistently with similar frameworks,[19,20] we attribute these spectral features to hybridization phenomena within the MOF, related to the formation of coordinative bonds. Specifically, predominantly occupied Fe 3d states hybridize with the lowest

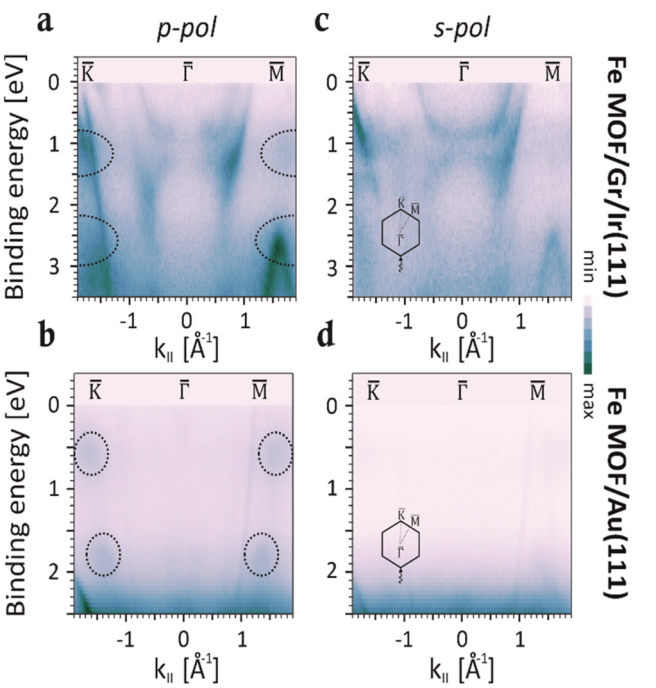

Fig. 4 Band maps along the high-symmetry direction $\bar{K}-\bar{\Gamma}-\bar{M}$ of the surface Brillouin zone of Gr/Ir(111) and Au(111) measured for: (a),(c) Fe MOF/Gr/Ir(111) and (b),(d) Fe MOF/Au(111) systems, using p- and s-polarized light, respectively.

unoccupied molecular orbitals (LUMO) of TCNQ, resulting in the formation of hybrid metal–organic states.[19] This interaction leads to the partial occupation of the LUMO through charge redistribution with Fe 3d states. This interpretation is further supported by complementary XAS data measured at the N K-edge, where quenching of the associated resonances is observed as the pristine TCNQ transitions into the Fe MOF structure (Fig. 2). Furthermore, we observe that the momentum distribution maps obtained with p-polarized light (Fig. 4a and b) exhibit higher intensity for the hybrid states compared to those with s-polarized light (Fig. 4c and d). This difference indicates the predominantly π-symmetric nature of the hybrid states, involving Fe 3d states and the MOs of the TCNQ ligands in the hybridization phenomena.

In addition, we synthesized Fe-TCNQ MOFs with varying Fe quantities. The spectra corresponding to 0.02 ML and 0.08 ML of total Fe coverage on the TCNQ layer on both Gr/Ir(111) and Au(111) substrates exhibit similar spectral line shapes (Fig. S4†). Hence, once the free coordination sites provided by the molecular layer are saturated, any additional Fe deposition is expected to result in the formation of metallic Fe clusters. Indeed, the spectrum corresponding to 0.08 ML of total Fe coverage is characterized by a notable shift in the main peak in the VB spectrum. This observation suggests that at 0.04 ML of total Fe coverage the saturation is reached, while additional Fe deposition (~0.08 ML) facilitates cluster formation, effectively doping the fully saturated Fe MOF structure. This mechanism accounts for the observed shift in spectral features without altering the overall spectral shape.

Conclusions

In conclusion, this study elucidates the intricate and complex interplay between coordinative bonding in 2D MOFs and the stabilization of HS states of Fe^{2+} in TCNQ-based frameworks. Our findings highlight that the interaction with the substrate results in a minimal effect on the magnetic properties of the MOFs, thus indicating the intrinsic and inherent robustness of these materials. This stability can be attributed to the strong coordinative interactions between the Fe 3d states and the π-symmetric MOs of the TCNQ ligands.

Experimental section

The Ir(111) single crystal was cleaned by argon ion (Ar^+) sputtering at room temperature, followed by annealing to 1500 K. The Au(111) single crystal underwent repeated cycles of Ar^+ sputtering and was subsequently annealed to 800 K. The sputtering was conducted at an energy of 1.5–2.0 keV.

Graphene was synthesized *via* chemical vapor deposition (CVD) using the ethylene (C_2H_4) gas. Ethylene was initially introduced into the preparation chamber at a pressure of 5×10^{-8} mbar for 2 minutes, after which the pressure was increased to 1×10^{-6} mbar for 5 minutes. The substrate temperature was maintained at 1400 °C during the growth process.

TCNQ was evaporated from a Knudsen-type evaporator at 410 K onto the substrate, which was kept at 300 K. We didn't observe the formation of a second layer of TCNQ on the substrate. Iron was evaporated from an e-beam evaporator operating at ion fluxes of 10 nA onto the TCNQ/Gr/Ir(111) and TCNQ/Au(111) interfaces and, after the Fe deposition, the samples were annealed to 475 K.

The photoemission measurements were conducted at the NanoESCA beamline of the Elettra synchrotron, using an electrostatic photoelectron emission microscope (PEEM) set-up described in detail in Ref. 26. Valence band spectra were collected at a photon energy of 30 eV with both p- and s-polarized light. A total energy resolution of 100 meV, which accounts for both the analyzer and beamline contributions, was found for the PEEM setup, while the momentum resolution was ±0.05 $Å^{-1}$. To prevent photon beam-induced damage and ensure the acquisition of high-quality data, the samples were rastered during the experiment. All measurements were performed at a pressure below 1×10^{-10} mbar, with the sample temperature maintained at 90 K.

XAS and XMCD measurements were conducted at the BOREAS beamline of the ALBA synchrotron.[31] Both XAS and XMCD spectra were collected in total electron yield mode at the N K-edge and Fe $L_{3,2}$-edges. The signal was normalized by the total electron yield measured on a diamond membrane placed between the last focusing mirror and the sample. In the XAS experiment, both Transverse Electric (s-polarization) and Transverse Magnetic (almost p-polarization) polarization experiments were performed by changing from linear vertical to linear horizontal polarizations. The XAS measurements were performed with the sample kept at 300 K to reduce substrate contributions to the background.

For the XMCD signals, obtained by subtracting the XAS spectra collected with positive helicity (I^+) from those with negative helicity (I^-) at the Fe $L_{3,2}$-edges, a magnetic field of B = 6 T and a temperature of approximately 5 K were used, with the magnetic field aligned with the direction of the incident light. To prevent beam-induced damage, the sample was continuously moved to expose fresh, non-illuminated areas.

Author contributions

Y. Y. G. Q. and V. F. performed the experiments and drafted the manuscript. All authors actively participated in the discussion of the results and the revision of the manuscript. S. M. and D. B. contributed to the valence band experiments. P. G. and M. V. provided significant assistance with the XAS and XMCD experiments.

Data availability

The data supporting this article have been included as part of the ESI.†

Conflicts of interest

There are no conflicts to declare.

Acknowledgements

This project received funding from the European Union's Horizon 2020 research and innovation program under grant agreement No 101007417, having benefited from the access provided by ALBA synchrotron in Barcelona, within the framework of the NFFA-Europe Pilot Transnational Access Activity, proposal ID499. Y. Y. G. Q. G. Z. and F. V. acknowledge the support from the Deutsche Forschungsgemeinschaft (DFG, German Research Foundation), Project ID 513136560. We thank D. Brandstetter, Dr A. Windischbacher and Prof. P. Puschnig for the fruitful discussion.

References

1 G. Gabarró-Riera and E. C. Sañudo, Challenges for exploiting nanomagnet properties on surfaces, *Commun. Chem.*, 2024, **7**, 1–11.
2 F. Donati, S. Rusponi, S. Stepanow, C. Wäckerlin, A. Singha, L. Persichetti, R. Baltic, K. Diller, F. Patthey, E. Fernandes, J. Dreiser, Ž. Šljivančanin, K. Kummer, C. Nistor, P. Gambardella and H. Brune, Magnetic remanence in single atoms, *Science*, 2016, **352**, 318–321.
3 K. Nagaoka, T. Jamneala, M. Grobis and M. F. Crommie, Temperature Dependence of a Single Kondo Impurity, *Phys. Rev. Lett.*, 2002, **88**, 077205.
4 M. Ternes, A. J. Heinrich and W. D. Schneider, Spectroscopic manifestations of the Kondo effect on single adatoms, *J. Phys.: Condens. Matter*, 2008, **21**, 053001.
5 P. Gambardella, S. Stepanow, A. Dmitriev, J. Honolka, F. M. F. De Groot, M. Lingenfelder, S. Sen Gupta, D. D. Sarma, P. Bencok, S. Stanescu, S. Clair, S. Pons, N. Lin, A. P. Seitsonen, H. Brune, J. V. Barth and K. Kern, Supramolecular control of the magnetic anisotropy in two-dimensional high-spin Fe arrays at a metal interface, *Nat. Mater.*, 2009, **8**, 189–193.
6 R. Gutzler, S. Stepanow, D. Grumelli, M. Lingenfelder and K. Kern, Mimicking Enzymatic Active Sites on Surfaces for Energy Conversion Chemistry, *Acc. Chem. Res.*, 2015, **48**, 2132–2139.
7 S. O. Parreiras, D. Moreno, B. Cirera, M. A. Valbuena, J. I. Urgel, M. Paradinas, M. Panighel, F. Ajejas, M. A. Niño, J. M. Gallego, M. Valvidares, P. Gargiani, W. Kuch, J. I. Martínez, A. Mugarza, J. Camarero, R. Miranda, P. Perna and D. Écija, Tuning the Magnetic Anisotropy of Lanthanides on a Metal Substrate by Metal–Organic Coordination, *Small*, 2021, **17**, 2102753.
8 S. O. Parreiras, C. Martín-Fuentes, D. Moreno, S. K. Mathialagan, K. Biswas, B. Muñiz-Cano, K. Lauwaet, M. Valvidares, M. A. Valbuena, J. I. Urgel, P. Gargiani, J. Camarero, R. Miranda, J. I. Martínez, J. M. Gallego and D. Écija, 2D Co-Directed Metal–Organic Networks Featuring Strong Antiferromagnetism and Perpendicular Anisotropy, *Small*, 2024, **20**, 2309555.
9 T. R. Umbach, M. Bernien, C. F. Hermanns, A. Krüger, V. Sessi, I. Fernandez-Torrente, P. Stoll, J. I. Pascual, K. J. Franke and W. Kuch, Ferromagnetic coupling of mononuclear Fe centers in a self-assembled metal-organic network on Au(111), *Phys. Rev. Lett.*, 2012, **109**, 267207.
10 J. Lobo-Checa, L. Hernández-López, M. M. Otrokov, I. Piquero-Zulaica, A. E. Candia, P. Gargiani, D. Serrate, F. Delgado, M. Valvidares, J. Cerdá, A. Arnau and F. Bartolomé, Ferromagnetism on an atom-thick & extended 2D metal-organic coordination network, *Nat. Commun.*, 2024, **15**, 1–8.
11 N. Abdurakhmanova, T. C. Tseng, A. Langner, C. S. Kley, V. Sessi, S. Stepanow and K. Kern, Superexchange-mediated ferromagnetic coupling in two-dimensional Ni-TCNQ networks on metal surfaces, *Phys. Rev. Lett.*, 2013, **110**, 027202.
12 D. Écija, J. I. Urgel, A. P. Seitsonen, W. Auwärter and J. V. Barth, Lanthanide-Directed Assembly of Interfacial Coordination Architectures-From Complex Networks to Functional Nanosystems, *Acc. Chem. Res.*, 2018, **51**, 365–375.
13 V. F. Yusuf, N. I. Malek and S. K. Kailasa, Review on Metal-Organic Framework Classification, Synthetic Approaches, and Influencing Factors: Applications in Energy, Drug Delivery, and Wastewater Treatment, *ACS Omega*, 2022, **7**, 44507–44531.
14 M. Wang, R. Dong and X. Feng, Two-dimensional conjugated metal–organic frameworks (2D c-MOFs): chemistry and function for MOFtronics, *Chem. Soc. Rev.*, 2021, **50**, 2764–2793.
15 Z. Jakub, A. Shahsavar, J. Planer, D. Hrůza, O. Herich, P. Procházka and J. Čechal, How the Support Defines Properties of 2D Metal-Organic Frameworks: Fe-TCNQ on Graphene versus Au(111), *J. Am. Chem. Soc.*, 2024, **146**, 3471–3482.
16 Z. Jakub, A. Kurowská, O. Herich, L. Černá, L. Kormoš, A. Shahsavar, P. Procházka and J. Čechal, Remarkably stable metal–organic frameworks on an inert substrate: M-TCNQ on graphene (M = Ni, Fe, Mn), *Nanoscale*, 2022, **14**, 9507–9515.
17 G. E. Pacchioni, L. Gragnaniello, F. Donati, M. Pivetta, G. Autès, O. V. Yazyev, S. Rusponi and H. Brune, Multiplet features and magnetic properties of Fe on Cu(111): From single atoms to small clusters, *Phys. Rev. B:Condens. Matter Mater. Phys.*, 2015, **91**, 235426.
18 C. Boeglin, S. Stanescu, J. P. Deville, P. Ohresser and N. B. Brookes, In-plane magnetocrystalline anisotropy observed on Fe/Cu(111) nanostructures grown on stepped surfaces, *Phys. Rev. B: Condens. Matter Mater. Phys.*, 2002, **66**, 014439.
19 S. Mearini, D. Baranowski, D. Brandstetter, A. Windischbacher, I. Cojocariu, P. Gargiani, M. Valvidares, L. Schio, L. Floreano, P. Puschnig, V. Feyer and C. M. Schneider, Band Structure Engineering in 2D Metal–Organic Frameworks, *Adv. Sci.*, 2024, **11**, 2404667.

20 D. Baranowski, M. Thaler, D. Brandstetter, A. Windischbacher, I. Cojocariu, S. Mearini, V. Chesnyak, L. Schio, L. Floreano, C. Gutiérrez, B. Os, P. Puschnig, L. L. Patera, V. Feyer and C. M. Schneider, Emergence of Band Structure in a Two-Dimensional Metal–Organic Framework upon Hierarchical Self-Assembly, *ACS Nano*, 2024, **18**, 39.

21 B. T. Thole, P. Carra, F. Sette and G. Van Der Laan, X-ray circular dichroism as a probe of orbital magnetization, *Phys. Rev. Lett.*, 1992, **68**, 1943.

22 P. Carra, B. T. Thole, M. Altarelli and X. Wang, X-ray circular dichroism and local magnetic fields, *Phys. Rev. Lett.*, 1993, **70**, 694.

23 S. Stepanow, A. Mugarza, G. Ceballos, P. Moras, J. C. Cezar, C. Carbone and P. Gambardella, Giant spin and orbital moment anisotropies of a Cu-phthalocyanine monolayer, *Phys. Rev. B:Condens. Matter Mater. Phys.*, 2010, **82**, 014405.

24 G. Van Der Laan and I. W. Kirkman, The 2p absorption spectra of 3d transition metal compounds in tetrahedral and octahedral symmetry, *J. Phys.: Condens. Matter*, 1992, **4**, 4189.

25 B. T. Thole and G. Van Der Laan, Branching ratio in X-ray absorption spectroscopy, *Phys. Rev. B:Condens. Matter Mater. Phys.*, 1988, **38**, 3158.

26 C. M. Schneider, C. Wiemann, M. Patt, V. Feyer, L. Plucinski, I. P. Krug, M. Escher, N. Weber, M. Merkel, O. Renault and N. Barrett, Expanding the view into complex material systems: From micro-ARPES to nanoscale HAXPES, *J. Electron Spectrosc. Relat. Phenom.*, 2012, **185**, 330–339.

27 T. C. Tseng, C. Urban, Y. Wang, R. Otero, S. L. Tait, M. Alcamí, D. Écija, M. Trelka, J. M. Gallego, N. Lin, M. Konuma, U. Starke, A. Nefedov, A. Langner, C. Wöll, M. Á. Herranz, F. Martín, N. Martín, K. Kern and R. Miranda, Charge-transfer-induced structural rearrangements at both sides of organic/metal interfaces, *Nat. Chem.*, 2010, **2**, 374–379.

28 G. Zamborlini, D. Lüftner, Z. Feng, B. Kollmann, P. Puschnig, C. Dri, M. Panighel, G. Di Santo, A. Goldoni, G. Comelli, M. Jugovac, V. Feyer and C. M. Schneider, Multi-orbital charge transfer at highly oriented organic/metal interfaces, *Nat. Commun.*, 2017, **8**, 1–8.

29 X. Yang, L. Egger, J. Fuchsberger, M. Unzog, D. Lüftner, F. Hajek, P. Hurdax, M. Jugovac, G. Zamborlini, V. Feyer, G. Koller, P. Puschnig, F. S. Tautz, M. G. Ramsey and S. Soubatch, Coexisting charge states in a unary organic monolayer film on a metal, *J. Phys. Chem. Lett.*, 2019, **10**, 6438–6445.

30 I. Cojocariu, H. M. Sturmeit, G. Zamborlini, A. Cossaro, A. Verdini, L. Floreano, E. D'Incecco, M. Stredansky, E. Vesselli, M. Jugovac, M. Cinchetti, V. Feyer and C. M. Schneider, Evaluation of molecular orbital symmetry via oxygen-induced charge transfer quenching at a metal-organic interface, *Appl. Surf. Sci.*, 2020, **504**, 144343.

31 A. Barla, J. Nicolás, D. Cocco, S. M. Valvidares, J. Herrero-Martín, P. Gargiani, J. Moldes, C. Ruget, E. Pellegrin and S. Ferrer, Design and performance of BOREAS, the beamline for resonant X-ray absorption and scattering experiments at the ALBA synchrotron light source, *J. Synchrotron Radiat.*, 2016, **23**, 1507–1517.

